Energy-dispersive measurements of the $K\alpha_3$, KM_1, $K\beta_1$, and $K\beta_2$ x-ray intensities relative to the $K\alpha_1$ intensity in lead and uranium

J. L. Campbell, P. L. McGhee, J. A. Maxwell, and R. W. Ollerhead
Guelph-Waterloo Program for Graduate Work in Physics, University of Guelph, Guelph, Ontario, Canada N1G 2W1

B. Whittaker
Chemistry Division, AERE Harwell, Oxfordshire OX11 ORA, England
(Received 14 August 1985)

Lead and uranium K x-ray spectra recorded with a specially designed Ge detector have been fitted using an accurately determined line-shape model. This provides the first accurate Ge measurements of the $K\alpha_3$ relative intensity and the first reported measurement of the KM_1 relative intensity. Measurements of the transition probabilities of $K\beta_1$ and $K\beta_2$ relative to the $K\alpha_1$ line provide a much more stringent test of calculated overlap and exchange effects than earlier ratios of gross line groups.

I. INTRODUCTION

In two recent papers[1,2] in this journal we have reported separate studies of relative transition probabilities (RTP's) within each of the $K\alpha$ and $K\beta$ x-ray multiplets in atoms within the atomic-number range $70 \leq Z \leq 92$. The experimental technique used was energy-dispersive spectroscopy via Ge(Li) and Ge solid-state detectors.

The first work[1] focused on determining the relative transition probability $I(K\alpha_2)/I(K\alpha_1)$ at the 1% precision level. Since it was the first energy-dispersive study to incorporate the intrinsic Lorentzian x-ray profile in the spectrometer resolution function, it also generated $K\alpha$ linewidths; although these had uncertainties of a few eV, their agreement with theory[3] lent credence to the nonlinear least-squares fitting methodology used to unravel overlapping x-ray peaks. More precise values have since been generated by wavelength-dispersive spectroscopy.[4,5] Finally, this work provided crude estimates of $I(K\alpha_3)/I(K\alpha_1)$, i.e., the ratio of the l-forbidden magnetic dipole line $(2S_{1/2}\text{-}1S_{1/2})$ to the dominant electric dipole line $(2P_{3/2}\text{-}1S_{1/2})$.

In our second paper[2] we reported the RTP's $I(K\beta_3)/I(K\beta_1)$, $I(K\beta_2)/I(K\beta_1)$, $I(KO_{23})/I(K\beta_1)$, $I(KP_{23})/I(K\beta_1)$, $I(K\beta_5)/I(K\beta_1)$, and $I(K\beta_4)/I(K\beta_1)$ within the $K\beta$ group. As Table I indicates, this group includes transitions from the M, N, O, and P shells to the K shell, whereas the $K\alpha$ group involves only the L and K shells. The results provided a significant improvement over previous data. As in the case of $I(K\alpha_2)/I(K\alpha_1)$ the various ratios exhibited smooth Z dependences and the ratios involving the strong electric dipole transitions agreed very well with Scofield's predictions, e.g., the RTP $I(K\beta_3)/I(K\beta_1)$ was within 1–2% of the Dirac-Hartree-Fock[6] (DHF) and the Dirac-Hartree-Slater[7] (DHS) predictions, which are almost equal. $I(K\beta_2)/I(K\beta_1)$, which involves the N_{23} and M_3 shells, agreed well with the DHF prediction, favoring it over the smaller DHS values; this preference for the DHF predictions, which include overlap and exchange effects, persisted in the results for $I(KO_{23})/I(K\beta_1)$ and $I(KP_{23})/I(K\beta_1)$ although these increasingly smaller ratios inevitably become less accurate than the M- and N-shell results. There was reasonable agreement with theory for the RTP's involving weak electric quadrupole transitions, and finally, in the case of uranium, there was a tentative and qualitative indication of the l-forbidden magnetic dipole KM_1 transition $(3S_{1/2}\text{-}1S_{1/2})$.

There remain two gaps in our attempt to test the existing calculations of K x-ray RTP's in heavy atoms to the limits of accuracy and precision afforded by Ge spectroscopy. It should first be feasible to improve greatly upon our estimates for the contributions of the magnetic dipole KL_1 ($K\alpha_3$) and KM_1 transitions; to do this is the main objective of this paper. All previously measured values for $I(K\alpha_3)/I(K\alpha_1)$ RTP's are by wavelength-dispersive spectroscopy and they vary from slightly below to over twice the theoretical values.[8]

The other gap arises from the fact that our $K\alpha$ and $K\beta$ multiplet studies[1,2] were entirely separate. We have not measured RTP's for major $K\beta$ lines relative to major $K\alpha$ lines. It was a systematic difference between the trend of many measurements of the gross ratio $I(K\beta)/I(K\alpha)$ and DHS theory[7] that originally led to the full DHF calculations,[6] which removed the discrepancy, at least within the

TABLE I. X-ray transition nomenclature.

KL_2	$K\alpha_2$	$K\alpha$
KL_3	$K\alpha_1$	
KM_2	$K\beta_3$	$K\beta_1'$
KM_3	$K\beta_1$	
KM_4	$K\beta_5$	
KM_5		
KN_2	$K\beta_2$	$K\beta_2'$
KN_3		
$KN_{4,5}$	$K\beta_4$	
KO_{23}		

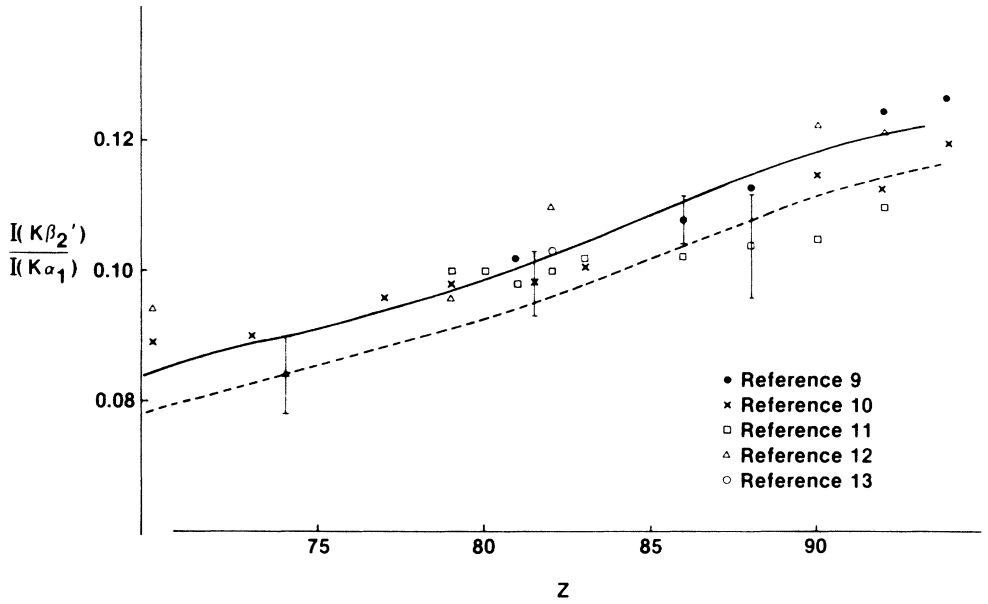

FIG. 1. Results of previous measurements of $I(K\beta_2')/I(K\alpha_1)$ ($Z \geq 70$) compared with DHF (solid line) and DHS (dashed line) predictions.

experimental errors. It would be of great interest to measure precisely whichever specific ratio $I(K\beta_i)/I(K\alpha_j)$ is most sensitive to the overlap and exchange effects treated in the DHF calculations. The two predictions differ by only 3% for $I(K\beta_1)/I(K\alpha_1)$, $I(KM_3)/I(KL_3)$, and $I(K\beta_3)/I(K\alpha_1)$ [i.e., $I(KM_2)/I(KL_3)$]. But when the shell separation increases, the difference is more dramatic, rising to 6% for $I(K\beta_2)/I(K\alpha_1)$ [i.e., $I(KN_{23})/I(KL_3)$]. Figure 1 reproduces the measurements[9–12] above $Z=70$ of $I(K\beta_2')/I(K\alpha_1)=I(KN_{23}+KO_{23}+KN_{45}+KP_{23})/I(K\alpha_1)$ from the review of Salem *et al.*,[14] and clearly the scatter is such as to preclude any useful conclusions; reported measurements do not separate $K\beta_2$ from $K\beta_2'$.

The present study fills these two gaps, using a new Ge spectrometer constructed to our design with this specific task in mind. The design minimizes low-energy peak distortions which detract from the quality of least-squares fits of analytic models to the x-ray spectra. Improvements were also made in the fitting methodology itself. Only two heavy atoms—lead and uranium—were used. As before, we did not see any need to measure at many Z values in view of the smooth Z dependences of the quantities of interest; moreover, we had observed in Ref. 2 that only at $Z \geq 80$ were our least-squares-fit results essentially free of a dependence upon starting parameters.

II. EXPERIMENTAL DETAILS

The lead x rays were derived from a radionuclide source of ^{207}Bi prepared by drying a droplet of a commercially supplied solution on a beryllium disk of 0.05-mm thickness.

The uranium x rays were obtained from radiochemically pure ^{235}Np prepared using previously reported cyclotron-irradiation and radiochemical-separation techniques.[15] ^{235}Np radiochemical purity was confirmed by γ- or x-ray and α-particle analysis, no other actinides or fission-product impurities being detected at the ppm level. Isotopic purity, determined by α-particle analysis, was estimated to be 99.999% by activity, the remaining 0.001% being assigned to ^{237}Np.

The ^{235}Np source was prepared by evaporation of a single drop of 4-molar hydrochloric-acid solution, centrally placed on a 0.02-mm-thick, 27-mm-diam Mylar backing foil. The dry deposit, approximately 4 mm in diameter, was fixed by applying a 10-mm-diam circle of adhesive Mylar.

The 200 mm$^2\times$10 mm intrinsic Ge crystal was mounted in a special cryostat by its manufacturer, Aptec Inc. (Toronto, Canada). The horizontal cryostat's beryllium window (0.5-mm thick) occupied its entire front face (diameter: 7.5 cm); in other words, the conventional aluminum endplate with a central beryllium window was replaced by a beryllium endplate. No attenuating material except the intervening air was placed between source and detector, and the source was held by fine nylon threads a few mm in front of the window. The objective of this design was to minimize Compton scattering of photons en route to the detector since this process is a major contributor to the approximately flat shelf observed on the low-energy side of full energy spectral peaks due to monoenergetic photons. The new detector, whose energy resolution was 530 eV at 122 keV, exhibited a shelf some 2—3 times less intense than in the devices we have previously used.[1,2]

Counting rates were kept below 1500 s^{-1} and both a pileup inspector (in the Ortec 572 amplifier) and a homemade pulse-shape inspector were used to suppress distorted pulses. The analog-to-digital converter (ADC) was a Nuclear Data 575 model equipped with a ND595 digital stabilizer and hosted by a Nuclear Data 66 pulse-

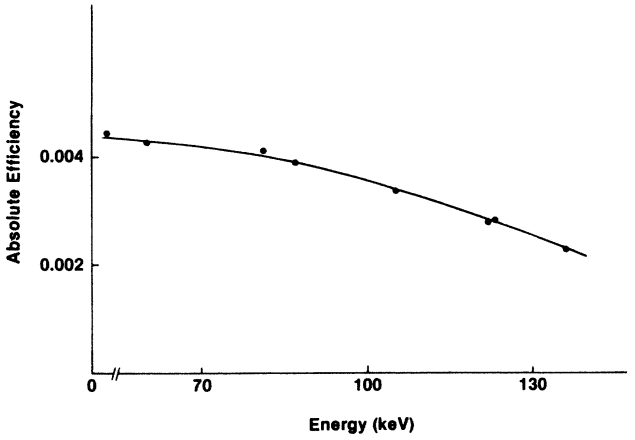

FIG. 2. Absolute efficiency of Ge detector.

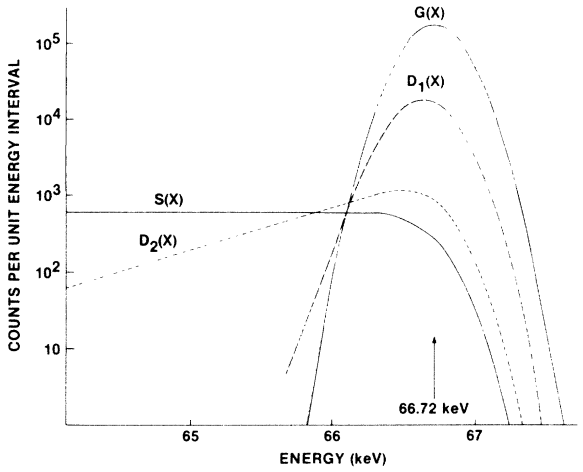

FIG. 3. Components of monoenergetic photon line shape at 66.7 keV.

height analyzer. In the uranium case over 90% of the counting rate was due to the predominant L x rays and so runs lasted from one to two weeks. The lead runs took one or two days.

Some auxiliary runs were done with lead and tin collimators to block the periphery of the Ge crystal, and some uranium runs were done with a 0.1-mm copper sheet to filter out the L x rays. These runs confirmed the results of the main runs and it is the latter which are reported here.

The detector's absolute efficiency in the energy region of interest was measured with radionuclide point-source standards of ^{241}Am, ^{57}Co (Physikalische-Technische-Bundesanstalt, Germany), and ^{133}Ba (Atomic Energy of Canada Ltd.), and the mixed standard 4275-10 supplied by the U.S. National Bureau of Standards. The efficiency curve is shown in Fig. 2; thanks to the increased detector thickness it varies less over either $K\alpha$–$K\beta$ span than any of our previous detectors, yielding a further improvement in precision.

The spectrometer's resolution function was obtained by recording spectra of monoenergetic γ rays from the radionuclides ^{241}Am, ^{171}Tm, ^{153}Gd, ^{109}Cd, and ^{57}Co. For each line, about 3×10^6 counts were recorded, whereas the $K\alpha$ and $K\beta$ intensities of Pb and U ranged from 2.5×10^6 to 60×10^6.

III. ANALYSIS OF THE γ-RAY DATA

A full description and justification of the analytical line shape $F(x)$ used to represent a γ-ray peak, i.e., of the resolution function, was given in our previous paper,[2] and need not be repeated. There was one necessary change. The low-energy exponential tail $D(x)$ had to be replaced by two tails $D_1(x)$ and $D_2(x)$ of very different slope. $D_1(x)$ was a steeply falling tail whose intensity clearly had to be associated with the main Gaussian component $G(x)$ in obtaining the peak area. $D_2(x)$ was a long-term tail falling slowly over a long energy interval left of the peak. The contributions of these, and of the flat Compton-scatter shelf $S(x)$, are shown for the 88.03-keV peak of ^{109}Cd in Fig. 3.

In Table II we indicate the goodness of fit and the two tail areas relative to their Gaussian parent, for the nonlinear least-squares fits of the model $S(x)$, incorporating a linear background $B(x)$. For the sake of uniformity we express all reduced chi-squared values (χ_r^2) throughout this paper as corresponding to an intensity of one million counts in the fitted region. This is easily shown[16] to be

$$\chi_r^2 = 1 + \frac{(\chi_r^2)_N - 1}{N}\ , \tag{1}$$

where $(\chi_r^2)_N$ is the actual chi squared achieved in fitting the measured spectrum containing N million counts. This approach eliminates potentially misleading comparisons of the goodness of fit for spectra of very different intensities.

A second round of fits was done to the γ-ray data using a quite different treatment of the background continuum. A background term was not included in the line-shape model. Instead, both the data and the peak model $S(x)$ were convoluted with a top-hat filter[17] before the fit was performed. This filter, shown in Fig. 4, when applied to a linear function reduces it to zero, and hence when it is applied to our data it should eliminate most of the quasilinear continuum (low-frequency component) while simply changing the shape of the peaks (high-frequency components). The chi-squared values lose their usual meaning

TABLE II. Reduced χ^2 (per 10^6 counts) and ratios of tail to Gaussian areas for monoenergetic γ-ray spectra.

Energy		$\frac{A(D_1)}{A(G)}$	$\frac{A(D_2)}{A(G)}$	$\frac{A(D_1)}{A(G)}$	$\frac{A(D_2)}{A(G)}$
(keV)	χ_r^2	Linear background		Filter fit	
59.54	1.028	6.90%	1.91%	11.0%	2.20%
66.72	1.053	11.45%	1.69%	12.85%	1.62%
88.03	1.078	6.05%	1.54%	13.80%	2.31%
103.18	1.025	9.90%	2.28%	8.96%	2.53%
122.10	1.072	7.41%	2.04%	10.6%	1.70%

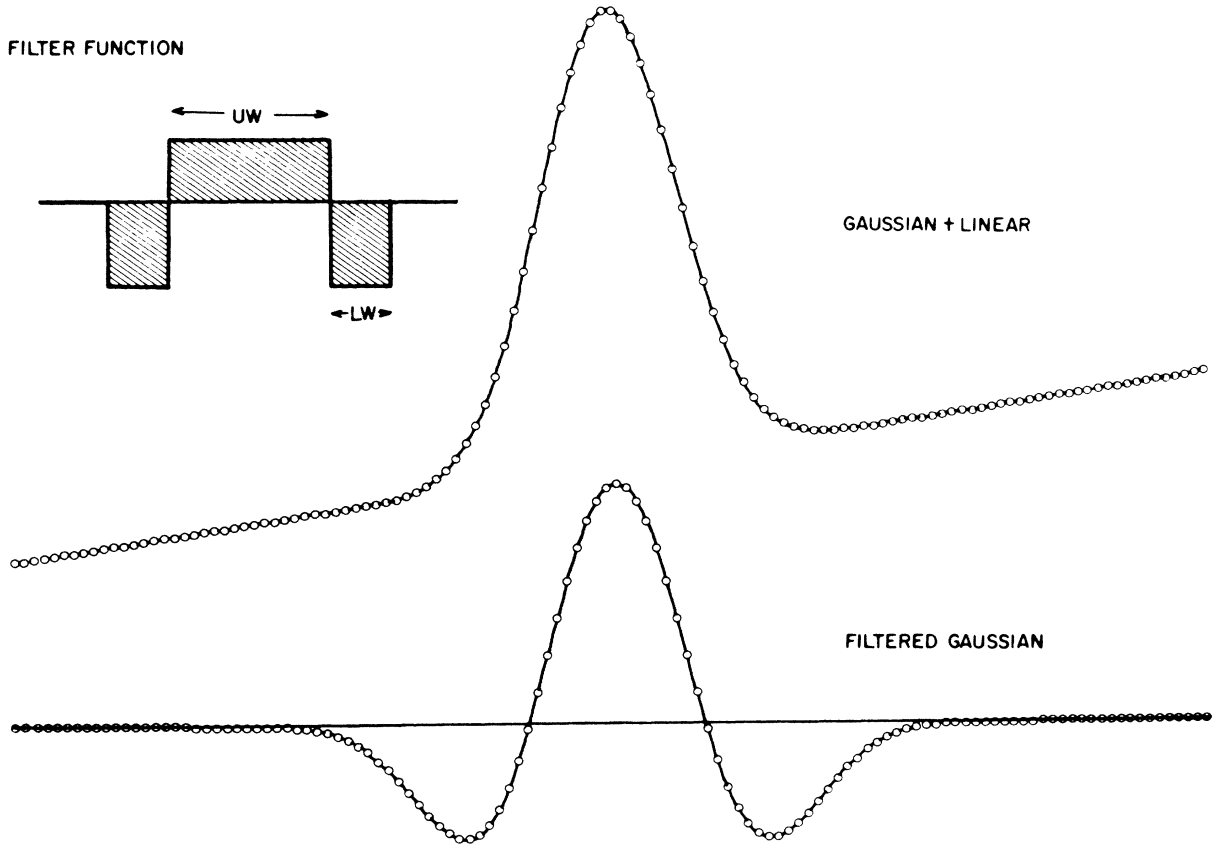

FIG. 4. Top-hat filter (Ref. 17). Convolution of the filter with the upper spectrum results in the lower spectrum where the linear background is removed. By permission of F. H. Schamber and Ann Arbor Science Publishers.

in this approach, but the quality of fit may be judged via the uniformity of the residues. The tail-area ratios are very similar, and the combined areas of the Gaussian and the short tail differ by typically 0.1% between the two methods. This second approach is extremely useful in fitting multiplets, as described in Sec. IV below.

The γ-ray fits established the appropriateness of the line-shape model. They also established bands of acceptable values for the low-energy tail parameters and, most importantly, for the tail-area fractions. The area fractions of Table II provide acceptance or rejection criteria for the x-ray multiplet fits, where there is a higher propensity for the fit to terminate in spurious minima. These may have acceptable χ_τ^2 values but they are identifiable by tail areas that are not within the bands established in Table II.

IV. ANALYSIS OF THE K X-RAY DATA

In contrast to all other reported K x-ray work with Ge detectors, our previous work[1,2] has taken account of the intrinsic Lorentzian x-ray line shape

$$L(x)=\frac{\Gamma/2\pi}{(X-X_0)^2+(\Gamma/2)^2}\ , \tag{2}$$

where Γ is the width of the line. The proper approach is to replace the γ-ray resolution function $F(x)$ by its convolute with $L(x)$. However, in our previous work we replaced

$$F(x)=G(x)+S(x)+D_1(x)+D_2(x) \tag{3}$$

by

$$K(x)=[G(x)\otimes L(x)]+S(x)+D_1(x)+D_2(x)\ , \tag{4}$$

i.e., we neglected convolution of the non-Gaussian components. This was done because convenient analytical approximations exist for the Voigtian function $L\otimes G$ and was justified by the minor role of the shelf and tail components. In the present context where the $K\alpha_3$ x-ray intensity is to be extracted from the low-energy edge of the $K\alpha_2$ line, this approximation had to be eliminated. Our current computer code employs a numerical method to perform the full convolution

$$K(x)=L(x)\otimes[G(x)+S(x)+D_1(x)+D_2(x)] \tag{5}$$

and this may be added to a linear background to complete the model or used in the continuum suppression mode.

All other aspects of the multiplet fitting methodology follow the detailed description of Ref. 2 and need not be discussed further. In the present work the "peak area" was the sum of the areas of the Gaussian and the short-term tail.

There were four principal spectral regions to be fitted,

TABLE III. Some results of fits to the lead and uranium $K\alpha$ and $K\beta$ x-ray spectra.

Multiplet	No. of lines	χ_r^2	Tail areas % $A(D_1)/A(G)$	$A(D_2)/A(G)$
		Linear background		
Pb $K\alpha$	3	1.05	5.9	2.3
Pb $K\beta$	9	1.07	8.0	2.35
U $K\alpha$	3	1.08	10.4	3.4
U $K\beta$	10	1.15	8.6	2.7
		Filtered background		
Pb $K\alpha$	3	1.01	8.2	2.0
Pb $K\beta$	9	1.08	9.4	2.9
U $K\alpha$	3	1.08	12.9	3.85
U $K\beta$	10	1.05	8.8	3.1

viz., the $K\alpha$ and $K\beta$ regions of both lead and uranium. Many fits were performed in each of these cases, with the linewidth Γ held fixed at a series of values in the vicinity of the theoretical values and the length of the fitted region varied; sometimes the short tail parameters were allowed to vary and sometimes they were fixed at the values expected from the γ-ray data. The best fits were obtained with Γ close to the predicted value. Table III summarizes some of the details of some of the fits chosen to generate the final results. As indicated earlier, other data were taken using collimators and absorbers; these were also fitted and the results supported those of the main experiment.

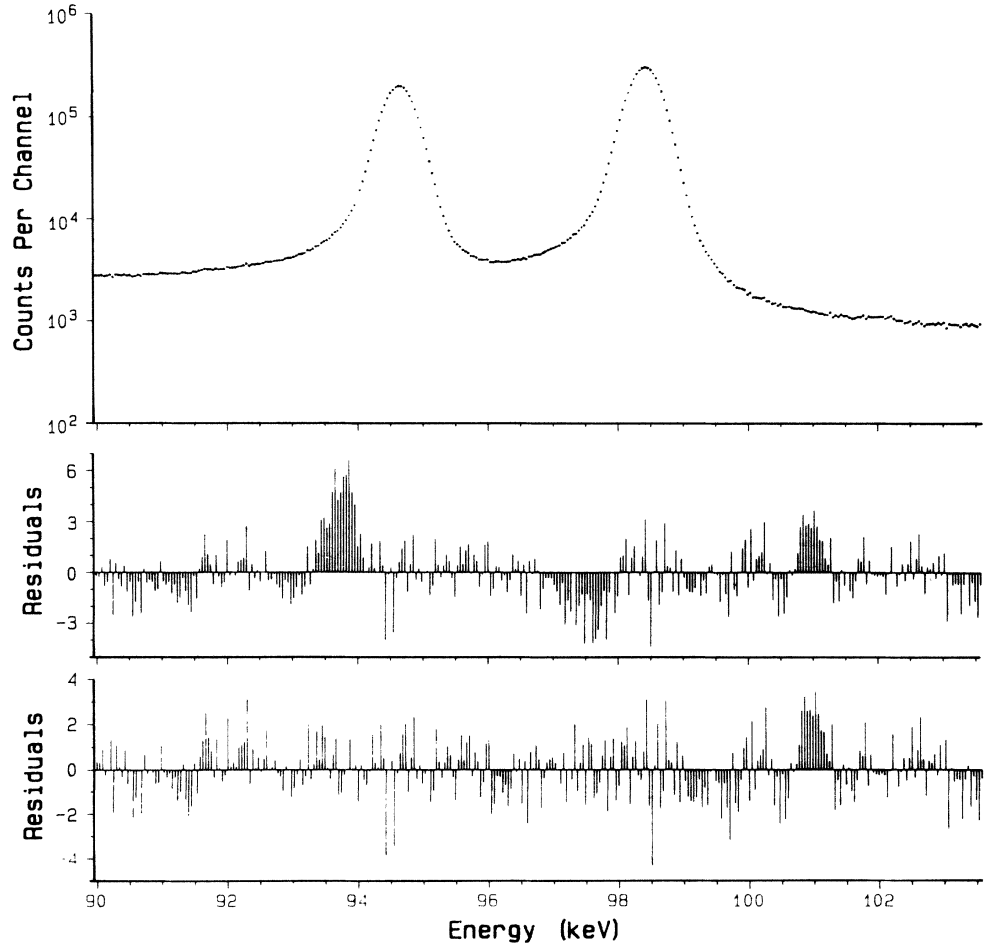

FIG. 5. Results of fit to the $K\alpha$ spectrum of uranium. (a) The $K\alpha_3$ line at 93.852 keV is excluded from the model and a strong residue appears at that energy. (b) $K\alpha_3$ is included in the model and the residue disappears.

TABLE IV. Relative transition probability $I(K\alpha_3)/I(K\alpha_1)$.

	$Z=82$	$Z=92$
Measured	$(1.02\pm0.2)\times10^{-3}$	$(2.3\pm0.3)\times10^{-3}$
Scofield calculation	0.98×10^{-3}	2.34×10^{-3}
Gabriel *et al.* calculation	0.98×10^{-3}	2.35×10^{-3}
Rosner and Bhalla calculation	0.91×10^{-3}	1.61×10^{-3}

V. RESULTS

A. $I(K\alpha_3)/I(K\alpha_1)$

When the 8.4×10^6-count uranium $K\alpha$ spectrum was treated using the top-hat filter technique, excellent fits were obtained with linewidths Γ of 96, 100, and 104 eV, and each case gave essentially the same RTP $I(K\alpha_3)/I(K\alpha_1)$ of $(2.31\pm0.02)\times10^{-3}$. The theoretical value of Γ is 104.5 eV. The fits with linear background gave more of a spread. Depending on the value of Γ and the actual length of the fitted region of the spectrum, the value of $I(K\alpha_3)/I(K\alpha_1)$ varied from 2.10×10^{-3} to 2.59×10^{-3}. The final result is $I(K\alpha_3)/I(K\alpha_1)=(2.3\pm0.30)\times10^{-3}$ at 90% confidence level.

To illustrate the role of the $K\alpha_3$ peak in the spectral fitting, Fig. 5 compares the residues in one particular fit, first with $K\alpha_3$ ignored and then with $K\alpha_3$ included in the model.

In the lead case the best fits were obtained with Γ values of 64, 66, and 68 eV, and when Γ was permitted to float, the result was $\Gamma=66.5$ eV. This excellent agreement with the theoretical value of 66.5 eV lends confidence in the results for $I(K\alpha_3)/I(K\alpha_1)$. In the 20×10^6-count spectrum with the uncollimated detector, there was only a slight small difference between the results of the two background treatments, giving a range $(1.06-1.21)\times10^{-3}$. However, when a tin collimator was used the result was $(0.84-0.87)\times10^{-3}$. The fitting indicated 1σ errors of about 7%. If we accept a mean $I(K\alpha_3)/I(K\alpha_1)=(1.02\pm0.2)\times10^{-3}$ all results are included and our claimed 2σ uncertainty (90% confidence level) is compatible with the errors of individual fits.

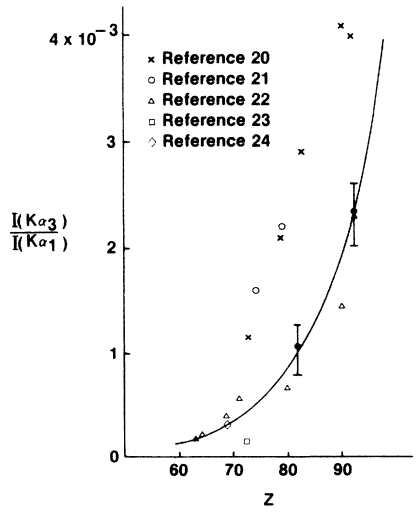

FIG. 6. Present and previous measurements of $I(K\alpha_3)/I(K\alpha_1)$, compared with the DHS predictions.

Table IV compares these results to Scofield's DHF predictions[6] and to the more recent calculations of Gabriel *et al.*[18] The latter derive analytic expressions for transition rates in the form of power series in an atomic scale parameter which characterizes a small-distance expansion of the screened relativistic potential. The table also includes older results of Rosner and Bhalla[19] obtained using DHS wave functions; we have extracted these from a plot in Ref. 19 via an epidiascope. The present results clearly favor Scofield's predictions.

Figure 6 adds our two results to the previous experimental information on $I(K\alpha_3)/I(K\alpha_1)$ given in the Salem *et al.*[14] review. Our results do not support the impression conveyed by the previous data that Scofield's predictions may be low.

B. $I(KM_1)/I(K\alpha_1)$ for uranium

To obtain useful information on the weak KM_1 transition a spectrum of very high intensity is needed. Since in the ^{235}Np source L x rays dominate the K x rays (by a factor 50:1) the only way to achieve this in an acceptance time was by the use of an 0.1-mm copper absorber. Figure 7 shows the results of fitting a $K\beta$ spectrum containing 13×10^6 counts. The evidence for the KM_1 line is not overwhelming, but the fit does indicate its presence, with $I(KM_1)/I(KM_3)=(4.5\pm1.1)10^{-3}$. This is in rather good agreement with Scofield's DHF prediction of 3.3×10^{-3}.

C. $I(K\beta_1)/I(K\alpha_1)$ and $I(K\beta_2)/I(K\alpha_1)$

The results for these two RTP's are given in Tables V and VI along with Scofield's DHF (Ref. 6) and DHS (Ref. 7) predictions. The uncertainties quoted are $\sim1.5-2$% at 90% confidence level; this is obtained simply by adding linearly the uncertainties in fitted peak areas plus any difference in the fractional areas of the long-term tails. This figure is compatible with the differences observed between the results given by the linear background and filtered background methods.

The mean results agree well with the DHF predictions. In the case of $I(K\beta_2)/I(K\alpha_1)$, measured here for the first time, there is a very strong demonstration of the overlap and exchange effects that are catered for in the DHF treatment. The $I(K\beta_2)/I(K\alpha_1)$ data are presented again in Fig. 8, which is to be compared with the preexisting situation shown in Fig. 1.

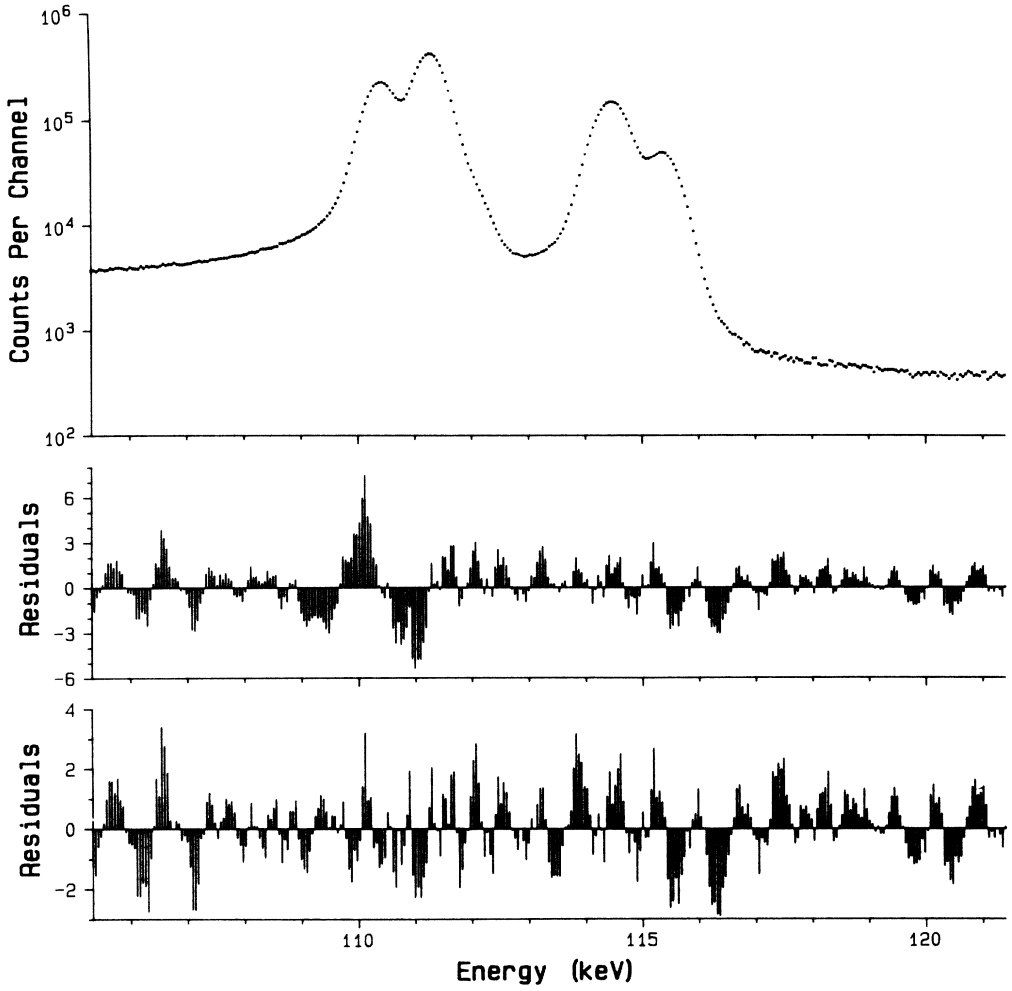

FIG. 7. Results of fit to uranium $K\beta$ spectrum. (a) The KM_1 line at 110.062 keV is excluded from the model and a strong residue appears at that energy. (b) KM_1 is included in the model and the residue disappears.

TABLE V. Relative transition probability $I(K\beta_1)/I(K\alpha_1)$. LB and FB denote linear background and filtered background methods, respectively.

	Experimental results			Theoretical	
Z	LB	FB	Mean	DHS (Ref. 6)	DHF (Ref. 7)
82	0.2223	0.2208	0.2215±0.003	0.2159	0.2225
92	0.235	0.227	0.231 ±0.004	0.2256	0.2313

TABLE VI. Relative transition probability $I(K\beta_2)/I(K\alpha_1)$. LB and FB denote linear background and filtered background methods, respectively.

	Experimental results			Theoretical	
Z	LB	FB	Mean	DHS (Ref. 6)	DHF (Ref. 7)
82	0.0836	0.0824	0.083±0.001	0.0789	0.0840
92	0.0944	0.0906	0.0925	0.0873	0.0923

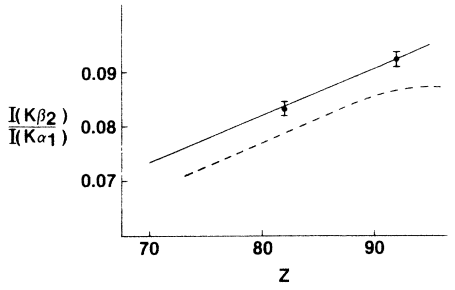

FIG. 8. Present measurements of $I(K\beta_2)/I(K\alpha_1)$ compared with DHF (solid line) and DHS (dashed line) predictions.

VI. CONCLUSIONS

We have concluded our Ge spectroscopic studies of the $K\alpha$ and $K\beta$ x-ray series at high Z by presenting the first quantitative Ge measurements of the RTP $I(K\alpha_3)/I(K\alpha_1)$ and by demonstrating excellent agreement of $I(K\beta_1)/I(K\alpha_1)$ and $I(K\beta_2)/I(K\alpha_1)$ with Scofield's Dirac-Hartree-Fock predictions. The work on $I(K\beta_2)/I(K\alpha_1)$ provides a more finely focused test of the overlap and exchange effects inherent in the DHF treatment than prior measurements of the gross RTP of the $K\beta$ and $K\alpha$ line groups.

In contrast to the prior wavelength-dispersive data, the present energy-dispersive data support the DHF calculations of $I(K\alpha_3)/I(K\alpha_1)$. Finally, we can now claim to have observed the $3S_{1/2}$-$1S_{1/2}$ transition and shown that $I(KM_1)/I(K\alpha_1)$ agrees with theory, albeit within large uncertainty limits.

We believe that any further refinement of relative transition probabilities to the K shell will have to come from wavelength-dispersive spectroscopy using intense x-ray sources along the lines described by Barreau *et al.*[5]

ACKNOWLEDGMENTS

Four of us (J.L.C., P.L.M., J.A.M., and R.W.O.) gratefully acknowledge the support of the Natural Sciences and Engineering Research Council of Canada.

[1]J. L. Campbell and C. W. Schulte, Phys. Rev. A **22**, 609 (1980).
[2]J. A. Maxwell and J. L. Campbell, Phys. Rev. A **29**, 1174 (1984).
[3]M. O. Krause and J. H. Oliver, J. Phys. Chem. Ref. Data **8**, 329 (1978).
[4]E. G. Kessler, Jr., R. D. Deslattes, D. Girard, W. Schwitz, L. Jacobs, and O. Renner, Phys. Rev. A **26**, 2696 (1982).
[5]G. Barreau, H. G. Börner, T. von Egidy, and R. W. Hoff, Z. Phys. A **308**, 209 (1982).
[6]J. H. Scofield, Phys. Rev. A **9**, 1041 (1974).
[7]J. H. Scofield, Phys. Rev. **179**, 9 (1969).
[8]J. H. Scofield, in *Atomic Inner-shell Processes,* edited by B. Crasemann (Academic, New York, 1975).
[9]W. D. Schmidt-Ott, F. Tolea, and R. W. Fink, in *Proceedings of the International Conference on Inner-Shell Ionization Phenomena and Future Applications* (USAEC Conference 720404), edited by R. W. Fink, S. T. Manson, J. M. Palms, and P. V. Rao (USAEC Technical Information Center, Oak Ridge, Tenn., 1973).
[10]J. H. McCrary, L. V. Singman, L. H. Ziegler, L. D. Looney, C. M. Edmonds, and C. E. Harris, Phys. Rev. A **4**, 1745 (1971).
[11]A. G. de Pinho, Phys. Rev. A **3**, 905 (1971).
[12]P. J. Ebert and V. W. Slivinsky, Phys. Rev. **188**, 1 (1969).
[13]J. S. Hansen, H. U. Freund, and R. W. Fink, Nucl. Phys. **A153**, 465 (1970).
[14]S. I. Salem, S. L. Panossian, and R. A. Krause, At. Data Nucl. Data Tables **14**, 91 (1974).
[15]B. Whittaker, Nucl. Instrum. Methods **223**, 531 (1984).
[16]J. L. Campbell, Int. J. Appl. Radiat. Isot. **33**, 661 (1982).
[17]F. H. Schamber, in *X-ray Fluorescence Analysis of Environmental Samples,* edited by T. G. Dzubay (Ann Arbor Science Publishers, Ann Arbor, Michigan, 1979).
[18]O. V. Gabriel, S. Chaudhuri, and R. H. Pratt, Phys. Rev. A **24**, 3088 (1981).
[19]H. R. Rosner and C. P. Bhalla, Z. Phys. **231**, 347 (1970).
[20]G. C. Nelson and B. G. Saunders, J. Phys. (Paris) Colloq. **32**, C4-97 (1969).
[21]O. Beckman, Ark. Fys. **9**, 495 (1955).
[22]O. W. B. Schult, Z. Naturforsch. **26A**, 368 (1971).
[23]R. K. Smither, M. S. Freedman, and F. T. Porter, Phys. Lett. **32A**, 405 (1970).
[24]F. Boehm, Phys. Lett. **33A**, 417 (1970).